



Cite this: *Nanoscale*, 2016, **8**, 18616

Received 22nd September 2016,  
 Accepted 13th October 2016

DOI: 10.1039/c6nr07504e

[www.rsc.org/nanoscale](http://www.rsc.org/nanoscale)

## Super-oxidation of silicon nanoclusters: magnetism and reactive oxygen species at the surface

Sergey Lepeshkin,<sup>\*a,b</sup> Vladimir Baturin,<sup>a,b</sup> Evgeny Tikhonov,<sup>b,c</sup> Nikita Matsko,<sup>a,b</sup> Yurii Uspenskii,<sup>a</sup> Anastasia Naumova,<sup>b,d</sup> Oleg Feya,<sup>b</sup> Martin A. Schoonen<sup>e</sup> and Artem R. Oganov<sup>b,d,f,g</sup>

**Oxidation of silicon nanoclusters depending on the temperature and oxygen pressure is explored from first principles using the evolutionary algorithm, and structural and thermodynamic analysis. From our calculations of 90 Si<sub>n</sub>O<sub>m</sub> clusters we found that under normal conditions oxidation does not stop at the stoichiometric SiO<sub>2</sub> composition, as it does in bulk silicon, but goes further placing extra oxygen atoms on the cluster surface. These extra atoms are responsible for light emission, relevant to reactive oxygen species and many of them are magnetic. We argue that the super-oxidation effect is size-independent and discuss its relevance to nanotechnology and miscellaneous applications, including biomedical ones.**

Silicon nanoparticles are promising for many applications including nanoelectronics, optoelectronics, solar cells, biomedical imaging sensors, *etc.* One of their unique properties, hinging on their reduced dimension, is photoluminescence with a tunable wavelength (size, shape and oxidation dependent), which is absent in bulk silicon.<sup>1</sup> As oxidation plays an important role in CMOS technology, its in-depth study in silicon particles is a key problem within nanotechnology research. Additional motivation for this study comes from the notion that small silica particles can induce health burden,<sup>2</sup> including the development of cancer, on one hand and be useful in drug delivery and therapy on the other.<sup>3</sup>

The exploration of Si–O clusters is also of interest for astrophysics and geophysics as it can bridge the gap between the

presence of SiO molecules in the circumstellar space and the dominance of silicate minerals in the Earth crust. The oxidation of silicon nanoobjects changes not only their composition, but affects the atomic structure as well. The existence of over 10 crystalline forms of silica illustrates the great diversity of configurations, which is expected in oxidized silicon clusters. Currently, the main body of structural information on clusters is provided by the methods of global optimization (see *e.g.* ref. 4), while experimental data are limited.<sup>5</sup> Earlier calculations focused on clusters with stoichiometric (SiO)<sub>n</sub> or (SiO<sub>2</sub>)<sub>n</sub> compositions.<sup>5,6</sup> Only a few studies addressed nonstoichiometric Si<sub>n</sub>O<sub>m</sub> clusters with  $m < 2n$  (see *e.g.* ref. 7 and 8), while clusters with  $m > 2n$  have never been considered.

In this Letter we explore oxidation trends in silicon clusters by performing a first-principles search for their optimal structures and applying a thermodynamical approach. Calculations were conducted for 90 Si<sub>n</sub>O<sub>m</sub> clusters with  $n \leq 10$  and  $0 \leq m \leq 2n + 9$ . The lowest-energy structures were found by the evolutionary algorithm (the USPEX code)<sup>9–11</sup> combined with density-functional calculations within the PAW-PBE approach<sup>12,13</sup> implemented in the VASP code.<sup>14,15</sup> Energies of the best structures were improved by the all-electron ORCA code<sup>16</sup> and the def2-TZVPP basis set.<sup>17</sup> These results are in good agreement with the ones for (SiO)<sub>n</sub>, (SiO<sub>2</sub>)<sub>n</sub>, and Si<sub>6</sub>O<sub>m</sub> clusters.<sup>5–8</sup> To show energy gains due to the O-atoms addition, we used reaction and transition energies:  $E_{\text{react}}(n,m) = E(\text{Si}_n\text{O}_m) - E(\text{Si}_n) - (m/2)E(\text{O}_2)$  and  $E_{\text{trans}}(n,m,m') = (E_{\text{react}}(n,m') - E_{\text{react}}(n,m)) / (m' - m)$  ( $n$  is omitted in the most discussed case  $n = 7$ ). By employing the ORCA code, we also calculated the vibrational spectra of Si–O clusters, which were used in thermodynamic analysis.

The most detailed calculations were performed for the Si<sub>7</sub>O<sub>m</sub> series, which was adopted as a model system. Fig. 1 presents the structures of Si<sub>7</sub>O<sub>m</sub> clusters with  $m = 0–23$  and the corresponding reaction energies. Successive oxidation is divided into four stages based on progressive changes in interatomic bonding: (I) Si–Si and Si–O bonds coexist in clusters, (II) Si–Si bonds disappear, while the number of Si–O–Si

<sup>a</sup>P.N. Lebedev Physical Institute, Russian Academy of Sciences, 119991 Leninskii prosp. 53, Moscow, Russia. E-mail: [lepeshkin@lpi.ru](mailto:lepeshkin@lpi.ru)

<sup>b</sup>Moscow Institute of Physics and Technology, Dolgoprudny, Moscow Region 141700, Russia

<sup>c</sup>Physics Department, Moscow State University, Leninskie Gory, Moscow 119991, Russia

<sup>d</sup>Skolkovo Institute of Science and Technology, Skolkovo Innovation Center, Nobel St. 3, Moscow 143026, Russia

<sup>e</sup>Brookhaven National Laboratory, Upton, NY 11793-5000, USA

<sup>f</sup>Department of Geosciences and Center for Materials by Design, Stony Brook University, Stony Brook, NY 11794, USA

<sup>g</sup>Northwestern Polytechnical University, Xi'an, Shaanxi 720072, PR China

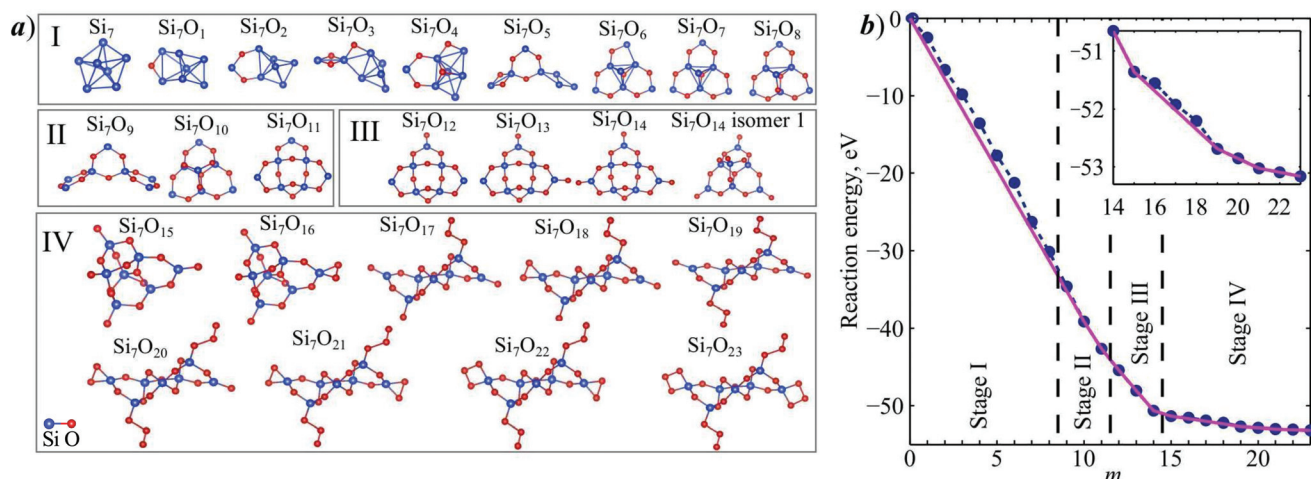


**Fig. 1** (a) Ground-state structures of  $\text{Si}_7\text{O}_m$  clusters from first-principles evolutionary calculations (structure of the 1st  $\text{Si}_7\text{O}_{14}$  isomer is also shown). The boxes correspond to four stages of oxidation. Blue and red circles denote, respectively, silicon and oxygen atoms. (b) Reaction energies of  $\text{Si}_7\text{O}_m$  clusters: calculated  $E_{\text{react}}(m)$  are shown by dots, an enveloping line goes through thermodynamically stable clusters.

bonds increases; (III) all Si–O–Si-positions are already filled, new O atoms occupy terminating positions with a single Si-neighbor; (IV) excess oxygen provides more and more numerous O–O bonds.

At the 1<sup>st</sup> oxidation stage ( $\text{Si}_7$  to  $\text{Si}_7\text{O}_8$ ), O atoms occupy bridging positions transforming Si–Si bonds into stronger Si–O–Si bonds. The Si–Si and Si–O–Si bonds are situated in different spatial regions (Fig. 1a), as was observed for  $(\text{SiO})_n$  clusters.<sup>6</sup> Segregation also occurs in the thermodynamic ensemble of  $\text{Si}_7\text{O}_m$  clusters with  $0 < m < 10$ , since the energy of the  $\text{Si}_7$ – $\text{Si}_7\text{O}_{10}$  cluster mixture (a solid line in Fig. 1b) is lower than the homogeneous ensemble energy of  $\text{Si}_7\text{O}_m$ . Segregation is caused by very different lengths of Si–Si and Si–O–Si bonds:  $d(\text{Si–Si}) \approx 2.5 \text{ \AA}$  and  $d(\text{Si–O–Si}) \approx 3.0 \text{ \AA}$ . When close to each other, these bonds greatly deform the structure and increase the cluster energy. Both intervals of  $m$ , where, on the one hand, Si–Si and Si–O–Si bonds coexist and, on the other, a homogeneous  $\text{Si}_7\text{O}_m$  ensemble is unstable, support this explanation.

At the 2<sup>nd</sup> stage ( $\text{Si}_7\text{O}_9$  to  $\text{Si}_7\text{O}_{11}$ ), Si–O clusters rearrange their structure to maximize the number of Si–O bonds (Fig. 1a). The formation of bridging bonds, which starts at the 1<sup>st</sup> stage and ends at the 2<sup>nd</sup> stage, is the strongest binding mechanism in Si–O clusters with a gain of  $E_{\text{trans}}(0,11) = -3.9 \text{ eV}$ . As further oxidation involves weaker bonding, the enveloping reaction energy has a notable kink at  $m = 11$  (Fig. 1b) that indicates an enhanced stability of  $\text{Si}_7\text{O}_{11}$ .

At the 3<sup>rd</sup> stage ( $\text{Si}_7\text{O}_{12}$  to  $\text{Si}_7\text{O}_{14}$ ), the dangling bonds of Si atoms (two bonds per O–Si–O fragment) are passivated by newly added O-atoms. This process is less favorable than bridging bond formation  $E_{\text{trans}}(11,14) = -2.7 \text{ eV}$ . Beginning from this point, oxidation turns to the cluster surface, where it is best described in terms of CGAs (Fig. 2). Because each CGA is linked to others by Si–O bonds, there are certain relationships between CGA numbers. In particular, the difference  $N(\text{CGA}\#4)$

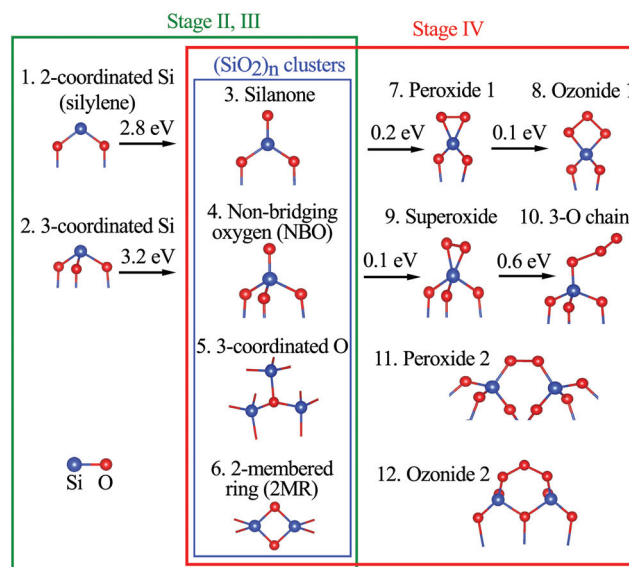


**Fig. 2** Characteristic groups of atoms (CGA) in Si–O clusters, arising at 2<sup>nd</sup> to 4<sup>th</sup> stages and their transition energies.

–  $N(\text{CGA}\#5)$  should be zero or an even integer. In terms of CGA, the 3<sup>rd</sup> stage is a sequential transition of silylenes (CGA#1) to silanones (CGA#3). The stage ends just at the stoichiometric  $(\text{SiO}_2)_7$  composition. As much weaker bonds (mostly of the O–O type) are formed at greater O concentrations, the enveloping reaction energy line has a strong kink at  $(\text{SiO}_2)_7$  (Fig. 1) that highly stabilizes these clusters against oxygen redistribution.

The 4<sup>th</sup> oxidation stage (super-oxidation,  $\text{Si}_7\text{O}_{15}$  to  $\text{Si}_7\text{O}_{23}$ ) starts with a global rearrangement – the  $\text{Si}_7\text{O}_{15}$  cluster differs greatly from  $\text{Si}_7\text{O}_{14}$ . All clusters of this stage exhibit magnetic behavior. Its origin is revealed by the criterion of magnetism

in nanoobjects.<sup>18</sup> To predict a magnetic transition, the criterion estimates energy gain of one electron transfer from HOMO↓ to LUMO↑ in a nonmagnetic cluster, taking into account a response of the remaining electrons. It gives  $\Delta E_m = E_{\text{magn}} - E_{\text{non-magn}}$  as:

$$\Delta E_m = \Delta_g + \frac{1}{2} \int \text{d}\mathbf{r} \text{d}\mathbf{r}' [\Delta\rho(\mathbf{r}) \hat{\epsilon}^{-1} (\hat{V}_C - \hat{I}_{\text{xc}}) \Delta\rho(\mathbf{r}')] - \frac{1}{2} \int \text{d}\mathbf{r} m^2(\mathbf{r}) I_m. \quad (1)$$

Here  $\Delta_g$  is the HOMO–LUMO gap,  $\Delta\rho(\mathbf{r}) = |\psi^{\text{LUMO}\uparrow}(\mathbf{r})|^2 - |\psi^{\text{HOMO}\downarrow}(\mathbf{r})|^2$  and  $m(\mathbf{r}) = |\psi^{\text{LUMO}\uparrow}(\mathbf{r})|^2 + |\psi^{\text{HOMO}\downarrow}(\mathbf{r})|^2$  are the changes in the electron and spin density respectively,  $\hat{\epsilon}^{-1}$  and  $\hat{V}_C$  are the inverse dielectric function and bare Coulomb interaction operators,  $-I_{\text{xc}}(\mathbf{r}) = \delta^2 E_{\text{xc}}(\rho, m) / \delta\rho^2(\mathbf{r})$  and  $-I_m(\mathbf{r}) = \delta^2 E_{\text{xc}}(\rho, m) / \delta m^2(\mathbf{r})$ . Eqn (1) shows that narrow  $\Delta_g$  and localization of  $m(\mathbf{r})$  promote magnetism. This very scenario is realized in Si<sub>7</sub>O<sub>14</sub> and Si<sub>7</sub>O<sub>15</sub> clusters (Fig. 3). The non-magnetic Si<sub>7</sub>O<sub>14</sub> cluster has  $\Delta_g = 3.4$  eV and  $|\psi^{\text{HOMO}\downarrow}(\mathbf{r})|^2$  and  $|\psi^{\text{LUMO}\uparrow}(\mathbf{r})|^2$  delocalized over all cluster, while the Si<sub>7</sub>O<sub>15</sub> cluster (in its non-magnetic state) has  $\Delta_g = 0.03$  eV and the HOMO density localized on three terminating O atoms of non-bridging oxygen (NBO), which occupy ~7% of the cluster volume (see Fig. 3c). For these clusters three r.h.s. contributions of (1) relating to  $\Delta_g$ ,  $V_C - I_{\text{xc}}$  and  $I_m$  are:  $\Delta E_m(\text{Si}_7\text{O}_{14}) = 3.40 + 3.42 - 1.08$  eV = +5.74 eV and  $\Delta E_m(\text{Si}_7\text{O}_{15}) = 0.03 + 0.10 - 2.99$  eV = -2.86 eV, where  $\hat{\epsilon}^{-1} \approx 0.5$  was used. They show that magnetism in Si<sub>7</sub>O<sub>15</sub> originates from a partially occupied group of levels related to NBO oxygen, which is situated in a wide energy gap between the valence and conduction bands. Such an electronic structure ensures both benefits: a narrow  $\Delta_g$  and a localized  $|\psi^{\text{HOMO}\downarrow}(\mathbf{r})|^2$ . This is true only if  $N(\text{CGA}\#4) - N(\text{CGA}\#5) \geq 2$  (Si<sub>7</sub>O<sub>15</sub> cluster), while in a compensated situation  $N(\text{CGA}\#4) = N(\text{CGA}\#5)$  (Si<sub>7</sub>O<sub>14</sub> 1<sup>st</sup> isomer), all

oxygen levels inside the gap are occupied (Fig. 3b). This increases  $\Delta_g$  to 2.1 eV, so the transition to the magnetic state becomes unfavorable.

Upon further oxidation (Si<sub>7</sub>O<sub>16</sub> to Si<sub>7</sub>O<sub>23</sub>) the oxygen of silanone (CGA#3) is replaced by a closed chain of O atoms (CGA#7 or CGA#8), while the oxygen of NBO (CGA#4) is substituted by a free-ending O-chain (CGA#10). Transition energies of this stage decrease monotonically with  $m$ :  $E_{\text{trans}}(14,15) = -0.70$  eV,  $E_{\text{trans}}(15,19) = -0.33$  eV,  $E_{\text{trans}}(19,21) = -0.17$  eV and  $E_{\text{trans}}(21,23) = -0.07$  eV, which agrees with CGAs energetics in Fig. 2. Si<sub>7</sub>O<sub>15</sub>–Si<sub>7</sub>O<sub>23</sub> clusters have the spin moment  $M_s = 2\mu_B$ , 90% of which is located on CGA#4 or CGA#10. Other CGAs, as well as the remaining cluster areas, are magnetically neutral and contribute negligibly to  $M_s$ . All CGAs related to the 4<sup>th</sup> oxidation stage of Si<sub>7</sub>O <sub>$m$</sub>  are free radicals (CGA#4, #9, and #10) or contain weak O–O bonds (CGA#7, #8, #11 and #12). Thus they can be referred to as reactive oxygen species (ROS) similar to H<sub>2</sub>O<sub>2</sub>, O<sup>2-</sup> and OH. There are several additional noteworthy aspects of CGAs in Fig. 2. Firstly, silylene (CGA#1) is typical of the 1<sup>st</sup>–3<sup>rd</sup> stages (2 to 13), while a two-membered ring (CGA#6) is common for Si–O clusters as it can replace the Si–O–Si bond at the penalty of strongly deviating O–Si–O angles. It was observed experimentally at the surface of amorphous silica films.<sup>5</sup> Secondly, CGA#2, #9 and #11–12 yield insignificant energy gains, therefore they are common in Si<sub>7</sub>O <sub>$m$</sub>  isomers.

Our analysis of oxidation stages in Si<sub>7</sub>O <sub>$m$</sub>  was conducted in terms of interatomic bonds, CGAs, and their energetics; therefore it is easily transferred to Si–O clusters of arbitrary size. The calculations for 66 Si <sub>$n$</sub> O <sub>$m$</sub>  clusters with  $n \leq 6$  and  $8 \leq m \leq 10$  support this generalization and reveal trends identical to those in Si<sub>7</sub>O <sub>$m$</sub> . This generalization raises a question of stage boundaries changing with  $n$ . According to our calculations, the 1<sup>st</sup> stage (Si <sub>$n$</sub>  to Si <sub>$n$</sub> O <sub>$n+k_1$</sub> ) is over at  $m = n + k_1$  with  $k_1(n)$  increasing monotonically as:  $k_1(4) = -1$ ,  $k_1(7) = +1$  and  $k_1(10) = +3$ . In large Si–O particles, where bulk contribution dominates, Si–Si bonds die away only near the SiO<sub>2</sub> composition, so  $k_1(n \rightarrow +\infty) \rightarrow n$ . The parameter  $k_2 \geq k_1$ , which determines the end of the 2<sup>nd</sup> stage (Si <sub>$n$</sub> O <sub>$n+k_1+1$</sub>  to Si <sub>$n$</sub> O <sub>$n+k_2$</sub> ), changes similarly to  $k_1(n)$ :  $k_2(4) = +2$ ,  $k_2(7) = +4$ ,  $k_2(10) = +6$  and  $k_2(n \rightarrow +\infty) \rightarrow n$ . Both stages are bulk-like, which gives a simple asymptotic estimate  $k_2 \approx n(1 - n^{-1/3})$ , which reasonably agrees with exact data at  $n \leq 10$ . The 3<sup>rd</sup> stage is over just at (SiO<sub>2</sub>) <sub>$n$</sub> . As the 3<sup>rd</sup> and 4<sup>th</sup> stages have a surface character, their asymptotic extents are  $\Delta m_3 \approx n^{2/3}$  and  $\Delta m_4 \sim n^{2/3}$ . For surfaces of bulk samples, being the extreme case of  $n = \infty$  we expect the appearance of the same CGAs that exist either in the ground-state or low-energy isomer structures of Si–O clusters. The specific type of oxygen termination may depend on the crystallographic indices of a surface and the allotropy of silica.

The most novel feature of Si <sub>$n$</sub> O <sub>$m$</sub>  relates to the super-oxidation (4<sup>th</sup>) stage. Small Si <sub>$n$</sub> O <sub>$2n+1$</sub>  clusters with  $n \leq 4$  consist of a two-membered ring chain, which has silanone and peroxide-1 at opposite chain ends. Further oxidation transforms silanone to peroxide-1 and peroxide-1 to ozonide-1. As has been discussed above, all CGAs related to silanone are magnetically neutral. For this reason all very small Si <sub>$n$</sub> O <sub>$m$</sub>  clusters (with

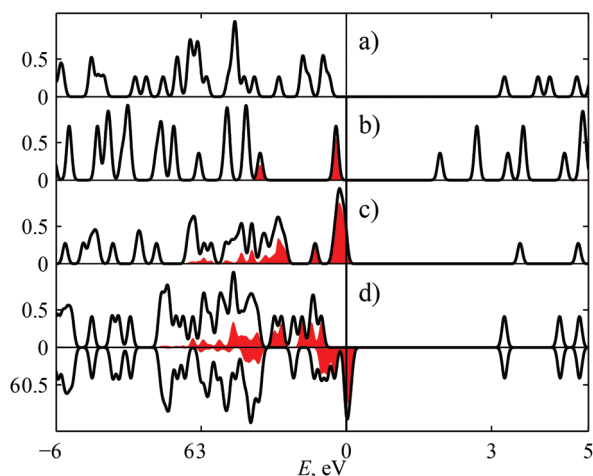


**Fig. 3** Electron densities of states broadened by a 0.05 eV Gaussian in Si<sub>7</sub>O<sub>14</sub> and Si<sub>7</sub>O<sub>15</sub> clusters: (a, b) Si<sub>7</sub>O<sub>14</sub> in the ground-state and 1<sup>st</sup> isomer configurations, (c, d) Si<sub>7</sub>O<sub>15</sub> in non-magnetic and magnetic states. Zero of energy corresponds to the Fermi level; the shaded areas show the contribution of NBO oxygen.

$n \leq 4$ , regardless of  $m$ ) are nonmagnetic. The formation of peroxide provides a small energy gain of 0.2 eV. To improve energetics,  $\text{Si}_5\text{O}_{11}$  realizes a different scenario—it structurally rearranges to form two non-compensated NBOs that yields a gain of 0.9 eV. Because of these NBOs,  $\text{Si}_5\text{O}_{11}$  is magnetic for the same reason as  $\text{Si}_7\text{O}_{15}$ . Similar scenarios are also realized in all  $\text{Si}_n\text{O}_{2n+1}$  with  $n \geq 6$ . In large  $\text{Si}_n\text{O}_m$  nanoclusters alternative (not ferromagnetic) spin ordering is possible that can affect magnetic properties. We did not address this problem, as the corresponding energy gain is small and weakly influences the thermodynamics and structure of clusters being the central subjects of our paper.

Considering the thermodynamics of  $\text{Si}_n\text{O}_m$ , we assumed that the system includes an ensemble of  $\text{Si}_n$  clusters and oxygen gas, which is characterized by a given number of  $\text{O}_2$  molecules ( $N_{\text{O}_2}$ ), pressure  $p$  and temperature  $T$ . The question is: what is the number of oxygen molecules bound to clusters in equilibrium and how are these molecules distributed among  $\text{Si}_n$  clusters? In general, the problem is reduced to minimization of the Gibbs free energy  $G(p, T)$  of the system. To perform this, we used two approaches. The first one assumes that the contribution of all clusters to  $G(p, T)$  is given by an enveloping line passing through  $g_{n,m}^{(0)}(T)$ , where  $g_{n,m}^{(0)}(T)$  are the Gibbs free energies of isolated  $\text{Si}_n\text{O}_m$  clusters in the ground-state configurations. The only free parameter is an amount of  $\text{O}_2$  molecules bound to clusters. Its variation determines the  $p$ - $T$  boundary between  $\text{Si}_n\text{O}_m$  and  $\text{Si}_n\text{O}_{m'}$  regions:

$$g_{\text{trans}}(n, m, m', T) = [\mu_{\text{O}_2}(p_a, T) + k_{\text{B}}T \ln(p/p_a)]/2. \quad (2)$$

Here  $g_{\text{trans}}(n, m, m', T)$  is the transition Gibbs free energy defined analogously to  $E_{\text{trans}}(n, m, m')$ . In addition to energy, it includes contributions from rotation and vibration of the clusters. The chemical potential of oxygen gas  $\mu_{\text{O}_2}(p_a, T) < 0$  corresponds to atmospheric  $\text{O}_2$  partial pressure, while  $p$ -dependence of  $\mu_{\text{O}_2}$  is shown explicitly. The  $p$ - $T$  phase diagram of  $\text{Si}_7\text{O}_m$  clusters obtained with (2) is shown in Fig. 4a. It is seen that

the stable  $\text{Si}_7\text{O}_m$  clusters with  $m < 14$  can exist only at very low  $p \leq 10^{-17}$  atm  $\approx 5 \times 10^{-17}$   $p_a$  and high  $T$ . Owing to their highest stability, the  $(\text{SiO}_2)_n$  clusters are in equilibrium with oxygen gas in a wide  $p$ - $T$  area, which includes elevated  $T$  and  $p \sim p_a$ . The clusters of the 4<sup>th</sup> oxidation stage arise in the diagram near  $p_a$  and  $T \leq 700$  K. This feature can be explained in approximation of  $E_{\text{trans}}(m, m') \approx g_{\text{trans}}(m, m', T)$ , where the  $T$ -dependent contribution of rotations and vibrations is neglected, as has been estimated for Mg-O clusters.<sup>19</sup> At the first three oxidation stages, when  $E_{\text{react}}(7, m) \approx -3$  eV, clusters are in equilibrium with oxygen gas only at high  $T$  (it makes  $\mu_{\text{O}_2}$  more negative) and  $p \ll p_a$ . At the 4<sup>th</sup> stage there is an approximate equality  $\mu_{\text{O}_2}(p_a, T = 150 \text{ to } 700 \text{ K}) \approx E_{\text{trans}}(m, m') \approx -0.1$  to  $-0.7$  eV, which explains why these clusters are predicted to exist under ambient conditions.

The second approach calculates the contributions of  $\text{Si}_n\text{O}_m$  clusters (in the ground-state and isomer configurations) to the thermodynamic ensemble. The variation of  $G(p, T)$  over the fraction of each configuration  $C_{n,m}^{(i)}(p, T)$  ( $i = 0$  and  $i \geq 1$  correspond, respectively, to the ground-state and isomer configurations) provides the Gibbs distribution:

$$C_{n,m}^{(i)}(p, T) = A(p, T) \exp \frac{-g_{n,m}^{(i)}(T) + m\mu_{\text{O}_2}(p, T)/2}{k_{\text{B}}T} \quad (3)$$

where  $A(p, T)$  is a normalizing constant. Fig. 4b shows contributions of  $\text{Si}_7\text{O}_m$  clusters to the ensemble, which were calculated with (3) at  $p = p_a$  and variable  $T$ . The distribution closely corresponds to the phase  $p$ - $T$  diagram of Fig. 4(a), but has smoothed  $T$ -boundaries. At most temperatures, two or more  $\text{Si}_7\text{O}_m$  clusters give significant contributions to the cluster ensemble, so, in general, the ensemble is non-uniform in composition.

The main features of the  $p$ - $T$  diagram and cluster distribution of  $\text{Si}_7\text{O}_m$  are directly linked to  $E_{\text{react}}(7, m)$ . As has been shown above, a general behavior of  $E_{\text{react}}(n, m)$  is defined by interatomic bonds and CGAs in clusters, which are nearly universal for Si-O clusters and vary from one oxidation stage to another. This fact determines the universal thermodynamic features of  $\text{Si}_n\text{O}_m$  clusters: (1) instability of clusters of the 1<sup>st</sup> stage; (2) occurrence of the 2<sup>nd</sup> and 3<sup>rd</sup> stage clusters, except for  $(\text{SiO}_2)_n$  ones, only at very low  $p$  and high  $T$ , as follows from  $E_{\text{trans}} \approx -3$  eV; (3) stability of  $(\text{SiO}_2)_n$  and a wide  $p$ - $T$  area of their existence; (4) low  $E_{\text{trans}}(n, m, m')$  of the 4<sup>th</sup> stage clusters and their equilibrium coexistence with pure oxygen gas at  $p \approx 0.21$  atm and  $T \approx 100$ –700 K. Actual atmosphere contains 1–3% of water vapor which may interact with the cluster surface. However, analysis of such processes requires the calculation of ternary Si-O-H nanoclusters which goes beyond the scope of our paper. The present consideration is based on equilibrium thermodynamics. In large silicon nanoparticles the 1<sup>st</sup> and the 2<sup>nd</sup> stages related to bulk oxidation may take enormously long time, so particles may exist in a nonequilibrium state with the pure silicon core and thin silica shell. Since the 3<sup>rd</sup> and 4<sup>th</sup> oxidation stages are of surface nature, they are the same as discussed above even if the total equilibrium is not reached.

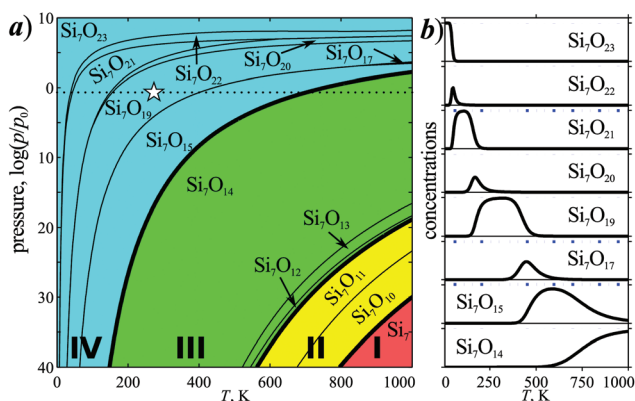


**Fig. 4** (a)  $p$ - $T$  phase diagram of  $\text{Si}_7\text{O}_m$  clusters ( $m = 0$ –23) under an oxygen atmosphere,  $p_0 = 1$  atm. with stages of oxidation shown by roman numerals. The standard conditions of oxygen ( $p_a \approx 0.21$  atm,  $T = 273$  K) are shown by a star symbol; (b) phase composition of  $\text{Si}_7\text{O}_m$  clusters ( $m = 0$ –23) at  $p_a$ .

These features are of key importance for the prediction and correct interpretation of Si–O cluster properties. In particular, instability and phase separation of the 1<sup>st</sup> stage Si–O clusters caused by a different length of Si–Si and Si–O–Si bonds is of interest for the formation of silicate minerals from circumstellar SiO molecules. The same mechanism explains oxide-assisted growth of long silicon nanowires, which goes through agglomeration of sub-oxide Si<sub>n</sub>O<sub>m</sub> ( $n \geq m$ ) clusters without a metal catalyst.<sup>20</sup> When pure Si and O-rich regions segregate in large Si–O nanoobjects, elastic strains push O-rich regions closer to the nanoobject surface, where their partial relaxation is possible. This picture agrees with the fact that the synthesized nanowires have a pure Si core and a silica shell of a few nanometers thickness.<sup>20</sup>

Another related problem is the photoluminescence of silica nanoparticles, which has been assigned to CGAs at the particle surface. Bright visible emission at  $h\omega = 1.99$  eV, 2.27 eV and 2.41 eV, which has been observed after annealing at  $T \approx 570$ –1170 K, was associated with NBO, silanone and peroxide-1.<sup>21–23</sup> Our analysis and the  $p$ – $T$  phase diagram of Si–O clusters indicate that this thermal treatment should form such emission centers as silanones and NBOs (of both compensated and non-compensated types), while the occurrence of peroxides and three-O chains (CGA#7 and #10) seems less probable.

According to our results, most Si–O clusters of the 4<sup>th</sup> stage exist in the spin-ordered state under ambient conditions. This finding can be of practical interest, because the search for magnetic materials compatible with silicon is among the challenging problems of spintronics.

Finally, this research provides new insights into the reactivity of silica in biological systems leading to toxicity at high exposure. As demonstrated here, super-oxidized (4<sup>th</sup>-stage) Si–O clusters possess ROS on their surface that remain stable under ambient conditions. These ROS groups are likely reactive toward biomolecules such as proteins, RNA and DNA, leading to oxidative stress and damage, ultimately resulting in disease (e.g., silicosis or lung cancer).<sup>24</sup>

This work was supported by Programmes of the Russian Academy of Sciences and Russian Foundation for Basic Research (grants 16-32-00922, 14-02-00583 and 16-02-00612), the Russian Science Foundation (grant 16-13-10459), the Foreign Talents Introduction and Academic Exchange Program (no. B08040) and the Project 5-100 grant to MIPT. Brookhaven National Laboratory is supported by the USDOE-Office of Science.

## References

- Z. Kang, Y. Liu and S.-T. Lee, *Nanoscale*, 2011, **3**, 777.
- J. Shi, H. L. Karlsson, K. Johansson, V. Gogvadze, L. Xiao, J. Li, T. Burks, A. Garcia-Bennett, A. Uheida, M. Muhammed, S. Mathur, R. Morgenstern, V. E. Kagan and B. Fadeel, *ACS Nano*, 2012, **6**, 1925–1938.
- F. Peng, Z. Cao, X. Ji, B. Chu, Y. Su and Y. He, *Nanomedicine*, 2015, **10**, 2109–2123.
- V. S. Baturin, S. V. Lepeshkin, N. L. Matsko, A. R. Oganov and Y. A. Uspenskii, *EPL*, 2014, **106**, 37002.
- C. R. A. Catlow, S. T. Bromley, S. Hamad, M. Mora-Fonz, A. A. Sokol and S. M. Woodley, *Phys. Chem. Chem. Phys.*, 2010, **12**, 786–811.
- S.-X. Hu, J.-G. Yu and E. Y. Zeng, *J. Phys. Chem. A*, 2010, **114**, 10769–10774.
- A. C. Reber, S. Paranthaman, P. A. Clayborne, S. N. Khanna and A. W. Castleman Jr., *ACS Nano*, 2008, **2**, 1729–1737.
- M. C. Caputo, O. Ona and M. B. Ferraro, *J. Chem. Phys.*, 2009, **130**, 134115.
- A. R. Oganov and C. W. Glass, *J. Chem. Phys.*, 2006, **124**, 244704.
- A. R. Oganov, A. O. Lyakhov and M. Valle, *Acc. Chem. Res.*, 2011, **44**, 227.
- A. O. Lyakhov, A. R. Oganov, H. T. Stokes and Q. Zhu, *Comput. Phys. Commun.*, 2013, **184**, 1172.
- P. E. Blöchl, *Phys. Rev. B: Condens. Matter*, 1994, **50**, 17953.
- J. P. Perdew, K. Burke and M. Ernzerhof, *Phys. Rev. Lett.*, 1996, **77**, 3865.
- G. Kresse and J. Furthmüller, *Phys. Rev. B: Condens. Matter*, 1996, **54**, 11169.
- G. Kresse and J. Furthmüller, *Comput. Mater. Sci.*, 1996, **6**, 15.
- F. Neese, *Wiley Interdiscip. Rev.: Comput. Mol. Sci.*, 2012, **2**, 73.
- F. Weigend and R. Ahlrichs, *Phys. Chem. Chem. Phys.*, 2005, **7**, 3297.
- Y. A. Uspenskii, E. V. Tikhonov and N. L. Matsko, *J. Magn. Magn. Mater.*, 2015, **383**, 100–103.
- S. Bhattacharya, S. V. Levchenko, L. M. Ghiringhelli and M. Scheffler, *Phys. Rev. Lett.*, 2013, **111**, 135501.
- R.-Q. Zhang, Y. Lifshitz and S.-T. Lee, *Adv. Mater.*, 2003, **15**, 635.
- A. S. Zyubin, Y. D. Glinka, A. M. Mebel, S. H. Lin, L. P. Hwang and Y. T. Chen, *J. Chem. Phys.*, 2002, **116**, 281.
- L. Vaccaro, A. Morana, V. Radzig and M. Cannas, *J. Phys. Chem. C*, 2011, **115**, 19476.
- L. Vaccaro, L. Spallino, S. Agnello, G. Buscarino and M. Cannas, *Phys. Status Solidi C*, 2013, **10**, 658–661.
- C. Albrecht, A. M. Knaapen, A. Becker, D. Höhr, P. Haberkettl, F. J. van Schooten, P. J. Borm and R. P. Schins, *Respir. Res.*, 2005, **6**, 129.